Available online at www.sciencedirect.com
SCIENCE DIRECT®
International Journal of Heat and Mass Transfer 47 (2004) 5059–5070
International Journal of HEAT and MASS TRANSFER
www.elsevier.com/locate/ijhmt

Transition boiling at jet impingement

Nathalie Seiler-Marie [a,b,*], Jean-Marie Seiler [c], Olivier Simonin [b]

[a] Électricité de France, Division Recherche et Développement, Département Mécanique des Fluides et Transferts Thermiques, 6 quai Watier, 78401 Chatou Cedex, France
[b] Institut de Mécanique des Fluides de Toulouse, UMR CNRS/INPT/UPS, avenue du Professeur Camille Soula, 31400 Toulouse, France
[c] CEA, Département de Thermohydraulique et de Physique, 17 rue des Martyrs, 38054 Grenoble Cedex 09, France

Received 23 January 2004; received in revised form 9 June 2004
Available online 10 August 2004

Abstract

The present paper is an attempt to summarize the results obtained on the modelling of the shoulder of flux phenomenon in the case of impinging jets on very hot plates. First, the phenomenon of shoulder of flux is described through literature results. Then, a physical approach of this phenomenon is given. The modelling of the shoulder of flux is based on the assumption of the existence of periodic bubble oscillations at the wall surface due to the jet hydrodynamic fragmentation. The modelling is carried out for the shoulder of flux region as well as for the first minimum and for the minimum film boiling points. These two points mark the beginning and the end of the shoulder of flux region.

Keywords: Impinging jet; Shoulder of flux; Heat transfer; Transition boiling

1. Introduction

Controlling the mechanical properties of steel products by means of a controlled cooling with a jet impingement on a very hot plate of steel is essential in particular in the metal processing industry. After being laminated, the steel strip has a temperature of about 1073–1273 K and is then cooled with water jets impinging on the moving strip. The basic mechanisms are not yet well understood. Indeed, well instrumented boiling experiments with impinging jet on very hot plates are difficult to perform because of technological problems.

However, some experiments of impinging jets on very hot plates have been carried out by a few authors. These experiments give precious informations on local phenomena occurring on the plate for the different boiling regimes: forced convection, nucleate boiling, transition boiling and film boiling.

Experiments have been performed in the configuration of an impinging jet on a hot plate show a characteristic behaviour of the boiling curve in the transition boiling regime. This phenomenon, called shoulder of flux, is characterized by a constant heat flux over a wide range of wall temperatures in the transition boiling regime (Fig. 1). Only few studies are available in the literature on boiling heat transfer in the configuration of an impinging jet on a hot plate and they mostly concern nucleate boiling and the critical heat flux (CHF). Thus,

* Corresponding author. Address: Électricité de France, Division Recherche et Développement, Département Mécanique des Fluides et Transferts Thermiques, 6 quai Watier, 78401 Chatou Cedex, France. Tel.: +33 4 42 27 18 92; fax: +33 4 38 78 52 51.
E-mail address: nathalie_seiler@hotmail.com (N. Seiler-Marie).

0017-9310/$ - see front matter © 2004 Elsevier Ltd. All rights reserved.
doi:10.1016/j.ijheatmasstransfer.2004.06.009

Nomenclature

C_p	liquid specific heat (kJ/(kg K))
d	nozzle diameter (m)
D	bubble diameter (m)
E	effusivity ($J^2/(K^2 m^4 s)$)
F	force (N)
F^a	aerodynamic force (N)
F^γ	gravity force (N)
g	gravitational acceleration (m/s^2)
h	distance between the jet and the heated plate (m)
h_{lg}	latent heat of vapourization (J/kg)
Ja	Jacob number (Eq. (28))
K'	a constant
K''	a constant
k	thermal conductivity (W/(mK))
M^*	non-dimensional number
P	pressure (Pa)
Q	flow rate of liquid displaced by instabilities (m^3/s)
q	heat flux (W/m^2)
R	bubble radius (m)
S	surface (m^2)
T	temperature (K)
t	time (s)
v	liquid velocity (m/s)
v_g^*	critical vapour velocity (m/s)
V	jet velocity (m/s)
y	vertical coordinate (m)

Greek symbols

α	thermal diffusivity (m^2/s)
ΔT	temperature difference (K)
ΔP	pressure difference (Pa)
δ	film thickness (m)
γ	jet induced acceleration (m/s^2)
γ_{tot}	total acceleration (m/s^2)
ρ	density (kg/m^3)
σ	surface tension (N/m)
τ	period (s)

Subscripts

A	point A
B	point B
crit	critical
g	gas, vapour
i	interface
j	at the impingement point
l	liquid
n	nozzle exit
MFB	miminum film boiling
sat	saturation
sh	shoulder
sub	subcooling
tot	total
w	wall

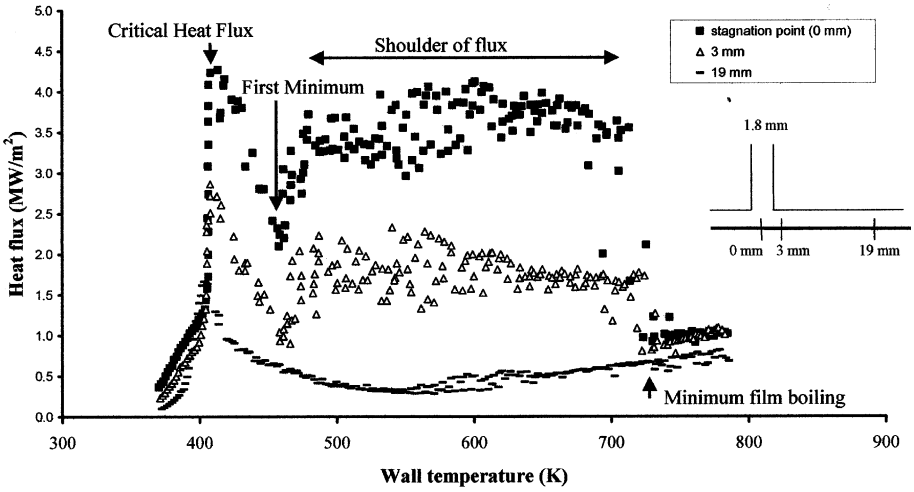

Fig. 1. Exchanged heat flux for different locations from the stagnation point of a planar water jet (Robidou [1] $V_j = 0.8$ m/s and $\Delta T_{sub} = 16$ K).

only few authors [1–5] reported observations on the shoulder of flux phenomenon and neither developed a phenomenological approach.

Only two steady-state studies on shoulder of flux are available in the literature. In these studies the heat flux is measured with constant wall temperature. Robidou et al. [6,7] carried out steady-state experiments along the entire boiling curve. The plate is cooled by an impinging vertical planar (1×9 mm^2) subcooled (5–16 K) water jet. The heater consists of eight modules of 10×10 mm^2 in order to avoid conduction heat transfer in longitudinal direction. The authors determine local boiling curves for different distances from the stagnation line of the planar jet, different jet velocity and different liquid subcooling. In the vicinity of the stagnation region the unusual shape of the boiling curve given by Fig. 1 has been observed. In transition boiling, for wall temperature greater than the CHF temperature, heat flux decreases as in a classical pool boiling system. A first heat flux minimum is reached for different wall temperatures depending on the distance to the stagnation line. Then, heat flux levels raise with increasing wall temperatures and reach different values depending on liquid subcooling, jet velocity and on the distance to the stagnation line. In the shoulder region, heat fluxes are then remarkably constant over a wide range of wall temperatures (500–700 K). The transition region ends with the film boiling regime at the miminum film boiling temperature. Miyasaka et al. [3], who measured the heat transfer from a very small surface (1.5 mm in hydraulic diameter) to an impinging planar jet of water (10×30 mm^2), observed an increase of heat flux with temperature after the CHF. Experiments were carried out at a jet temperature of 288 K and for jet velocities ranging from 1 to 15.3 m/s. The boiling curve in the transition region, after the CHF, could be divided into two transition regimes. The first one is characterized by a small increase of the heat flux with the surface temperature, whereas the second one exhibits an almost constant heat flux.

The other studies with impinging jets in transition boiling regime have been limited to transient quenching. Hall et al. [4] performed experiments under transient conditions starting from very high wall temperatures. The velocity of the circular water jet (5.1 mm in diameter) is 3 m/s at the nozzle exit and the liquid subcooling is $\Delta T_{sub} = 75$ K. Ishigai et al. [2] investigated the influence of liquid subcooling (5–55 K) and jet velocity (1–3.17 m/s) on the boiling curves. Heat flux shoulders are shifted to higher heat fluxes and wall temperatures as the liquid subcooling and jet velocity increase. Finally, Ochi et al. [5] carried out quenching experiments with a constant jet velocity (3 m/s) but with different liquid subcoolings (5–80 K) and nozzle diameters (5–20 mm).

2. Model developed for the heat flux in the "shoulder regime"

Starting from the analysis of Robidou's [1] experimental data presented in Fig. 2, we notice that the heat flux corresponding to the shoulder is in first approach proportional to liquid subcooling. This observation

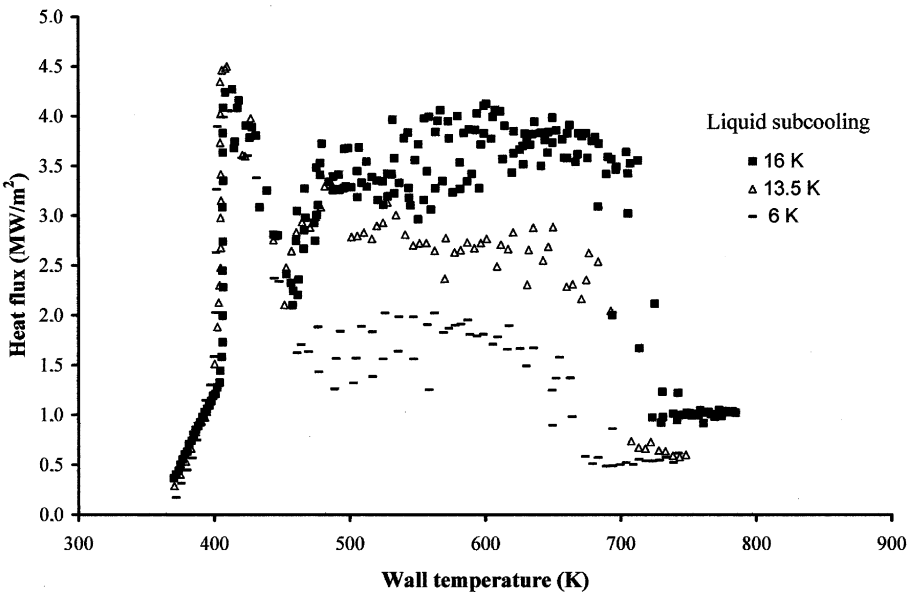

Fig. 2. Heat flux at the stagnation point for different liquid subcoolings ($\Delta T_{sub} = T_{sat} - T_l$, Robidou [1] $V_j = 0.8$ m/s).

leads us to the following interpretation: heat transfer in the shoulder region is mainly related to the heating up of the liquid and not to its vapourization. According to Engelberg-Forster and Greif [8], who carried out studies in nucleate boiling regime, the main heat transfer is obtained in this boiling regime by warming up of subcooled liquid. The displacement of hot liquid due to the production of vapour seems to be the predominant heat transfer mechanism in this boiling regime. By analogy, the idea was that the heat flux shoulder could arise from an unsteady phenomenon during which subcooled liquid is heated when it comes into contact with the hot plate and is then displaced into the bulk flow by bubble growth. As the heat flux corresponding to the shoulder decreases with the distance to the stagnation line (Fig. 1), instabilities, which are at the origin of such phenomenon, are thought to be related to the local jet hydrodynamics. The physical modelling considers the Rayleigh–Taylor instabilities at the liquid/vapour interface which originate in the deceleration region of the jet flow. The instabilities lead to vapour spots fragmentation and to periodic rewetting of the heated plate. This explanation of boiling mechanism in the heat shoulder region is supported by the interpretation of Robidou et al. [6,7]. Beyond CHF, the boiling is characterized by small vapour spots that result from bubble coalescence. Hence, the overall heat flux decreases towards the first minimum heat flux with the increasing wall temperature because of increasing size of vapour spots. Robidou et al. assume that in this boiling region, the jet is not strong enough to break the vapour spots. They think that vapour spot fragmentation suddenly happens at the first minimum: the break down of vapour spots would create a better—spray type—wetting of the surface leading to higher heat fluxes. This explanation is supported by the fact that the region between the CHF and the first minimum disappears with increasing jet velocity and, hence, with the jet force which leads to vapour spot breaking.

In a first subsection, the origin of such vapour spots fragmentation is described and the main features of this phenomenon (average vapour spot radius, oscillation period) are given. In a second subsection relation for the heat flux shoulder is derived from this physical approach.

2.1. Origin of vapour spot fragmentation

Rayleigh–Taylor instabilities occur at liquid/vapour interface when the stratification is submitted to a transverse pressure gradient. In Fig. 3, we consider a vapour layer which isolates the heated wall from a subcooled liquid layer before any instability is developed at the liquid/vapour interface. At the vapour/liquid interface both phases have low normal velocities. In pool boiling without impinging jet, Rayleigh–Taylor instabilities occur

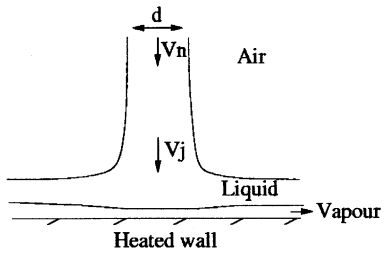

Fig. 3. Sketch of a jet impinging perpendicularly to a heated plate.

owing to gravitational acceleration which creates a force on the heavy fluid [9]. Hence, this fluid tends to penetrate into the underneath light vapour layer, so destabilizing the interface. In an impinging jet configuration, a source of instabilities at the liquid–vapour interface is added to the one due to the gravitational force. Indeed, the liquid jet deceleration is inducing also a pressure gradient which can be characterized by an equivalent acceleration γ. This jet deceleration is approached by Eq. (1)

$$\gamma = \frac{V_j^2}{d} \tag{1}$$

where V_j (m/s) is the impinging jet velocity near the stagnation point and d (m) the jet hydraulic diameter (Fig. 3) which is equal to the jet diameter in the case of a circular jet. As we consider the gravitational acceleration as well as the acceleration due to the jet hydrodynamics, the total acceleration becomes: $\gamma_{tot} = \gamma + g$. We assume that the vapour spot diameter under the jet cannot be greater than Rayleigh–Taylor's critical wavelength. This critical diameter is given by Eq. (2).

$$D_{crit} \sim 2\pi\sqrt{\frac{\sigma}{\gamma_{tot}(\rho_l - \rho_v)}} \tag{2}$$

The relation (2) expresses a competition between forces due to surface tension and the jet hydrodynamics. As long as the spot is smaller than the critical value given by Eq. (2), the surface tension force is predominant and the jet is not strong enough to break the spot down. But, beyond this critical value, the surface tension force is no longer predominant and the vapour spots are fragmented by the jet. The diameters of the spots are supposed to be constant, proportional to this critical value. The average period (τ) of vapour spot fragmentation is deduced from the observation of the following characteristic time scales:

- The bubble oscillation time scale with driving pressure (ΔP_l) proportional to $\gamma R_{crit}\rho_l$.

$$\tau_1 \sim R_{crit}\sqrt{\frac{1}{\gamma_{tot}R_{crit}}} \tag{3}$$

Eq. (3) is derived from a non-dimensional analysis.

$$\Delta P_1 \sim \rho_l \frac{R_{crit}^2}{\tau^2} \quad (4)$$

ΔP_1 is the pressure fluctuation created by the jet impingement. It may be approached by $\Delta P_1 = \frac{F}{S}$, with F (N/m^2) the force exerted by the jet on a vapour bubble and S (m^2) the application surface of this force; i.e. proportional to the bubble surface $\sim 4\pi R_{crit}^2$. F could be estimated as $\sim \pi D_{crit}^3 \rho_l \gamma_{tot}/6$ by considering the fluid acceleration in the volume occupied by characteristic bubble.

- The liquid travel time scale over a distance D_{crit} associated to a characteristic acceleration γ_{tot}.

$$\tau_2 \sim \sqrt{\frac{D_{crit}}{\gamma_{tot}}} \quad (5)$$

- The eviction time scale of a liquid column of height D_{crit} under a driving pressure $\Delta P_2 \sim \frac{\sigma}{R_{crit}}$.

$$\tau_3 \sim D_{crit}\sqrt{\frac{\rho_l R_{crit}}{2\sigma}} \quad (6)$$

The characteristic pressure difference (ΔP_2) is created in a bubble of critical radius (R_{crit}). This pressure difference drives the eviction of the liquid column above the growing bubble.

We notice that these three characteristic time scales depend on the same physical variables. It is notice worth to mention that these three time scales are of the same magnitude if we consider the relation (2) for D_{crit} (Eq. (7)).

$$\tau \sim \sqrt{\frac{R_{crit}}{\gamma_{tot}}} \sim \sqrt{\frac{D_{crit}}{\gamma_{tot}}} \sim D_{crit}\sqrt{\frac{\rho_l R_{crit}}{2\sigma}} \quad (7)$$

The fact that these three time scales are of same magnitude seems to be a requirement for the periodicity of bubble oscillation for the shoulder regime to be sustained. So, when a volume of liquid penetrates into the vapour, another liquid volume may be ejected by vapour emergence near to this location.

The order of magnitude of the period of bubble fragmentation is found by introducing relation (2) into relation (7). This corresponds in fact to the characteristic time scale associated to the Rayleigh–Taylor instabilities [10].

$$\tau \simeq \frac{\sigma^{1/4}}{(\rho_l - \rho_v)^{1/4}\gamma_{tot}^{3/4}} \quad (8)$$

2.2. Modelling of the heat flux in the shoulder region

Fig. 4 illustrates the hypothesized mechanism. At each bubble oscillation, a constant amount of liquid flows into the vapour and reaches the wall (sketch b in Fig. 4). This amount of liquid spreads on the wall. It is heated up by transient conduction (sketch c). When the average liquid temperature nearly reaches its saturation temperature, a part of this liquid, that directly touches the hot plate, is evaporated. The vapour generated evicts the hot liquid from the wall. This liquid is finally evacuated to the bulk of the flow (sketch d in Fig. 4). We assume that the heat transfer associated to the vapour generation is negligible and that the heat flux is mainly controlled by periodic ejection of heated liquid.

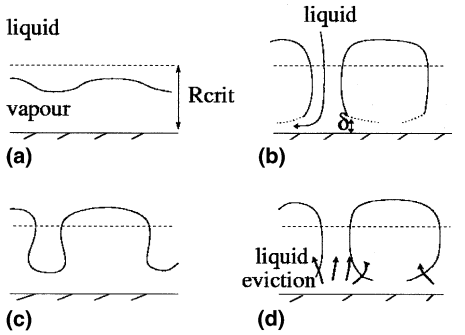

Fig. 4. Sketch of local phenomena leading to the heat flux shoulder.

The heat flux transferred by this mechanism (q_{sh} in W/m^2) is given by

$$q_{sh} = \rho_l C_{pl} \Delta T_{sub} \frac{Q}{S} \quad (9)$$

where ΔT_{sub} (K) is the liquid subcooling ($\Delta T_{sub} = T_{sat} - T_l$, where T_{sat} and T_l are the saturation and the bulk liquid temperature respectively). Q (m^3/s) is the flow rate of liquid pushed by bubble oscillations that reaches the heated wall. S (m^2) is the considered surface of the plate affected by bubble oscillations. We assume that the characteristic volume of liquid displaced by a single bubble (V) is proportional to the volume corresponding to the critical diameter (Eq. (2)).

$$V = K\frac{\pi D_{crit}^3}{6} \quad (10)$$

with K a constant such as $0 < K \leqslant 1$. This volume is displaced during period τ such that $Q = V/\tau$. The wall surface associated with a single bubble is taken as $S = \pi D_{crit}^2$. Finally, by combining previous relations we get Eq. (11) for the heat flux shoulder.

$$q_{sh} \sim K'\rho_l(\rho_l - \rho_v)^{-1/4}\sigma^{1/4}C_{pl}\Delta T_{sub}\gamma_{tot}^{1/4} \quad (11)$$

We obtain the value of K' from the 35 experimental data of Robidou [1] ($0.64 \leqslant V_j \leqslant 0.96$ m/s, $5 \leqslant \Delta T_{sub} \leqslant 19$ K, $d = 1.8$ mm). We find an average value for K' of 0.15 with a deviation of 0.013. Eq. (11) can be written after adjusting K' on Robidou's data at jet impingement:

$$q_{sh} = 0.15\rho_l(\rho_l - \rho_v)^{-1/4}\sigma^{1/4}C_{pl}\Delta T_{sub}\gamma_{tot}^{1/4} \quad (12)$$

Table 1
Experimental conditions and relative prediction error for the shoulder of flux at the stagnation point (fluid:water)

	Data number	d, mm	V_j, m/s	ΔT_{sub}, K	q_{sh}exp, MW/m^2	Relative error, %	Deviation, %
Robidou [1]	35	1.8	0.57–0.96	5–17	1.49–4.8	13.2	9.4
Miyasaka et al. [3]	3	10	1.4–15.3	85	30–58	22.5	19.9
Hall et al. [4]	1	5.1	3.31	75	35	34.4	
Ishigai et al. [2]	10	11	1.14–3.21	5–55	2.5–12	18.2	13.9
Ochi et al. [5]	8	5–20	3.08	5–80	1.5–9	69.3	40.1

2.3. Validation of the modelling

We compare the heat flux corresponding to the shoulder issued from the literature studies to the heat flux calculated with Eq. (12). In Table 1, one can observe the different experimental data for heat flux shoulder as well as the relative error and deviation. The calculated heat flux (Eq. (12)) is also plotted versus the measured heat flux in Fig. 4. By considering the results reported in Table 1 and in Fig. 5, we conclude that Eq. (12) correlates experimental results available in the literature (obtained either in steady-state or in transient regime) with a deviation of approximately ±20% except for Ochi et al.'s results (Fig. 5).

As for experimental conditions reported in Table 1, the gravitational acceleration g is negligible compared to γ, so $\gamma_{tot} \simeq \gamma$ and relation (12) becomes:

$$q_{sh} = 0.15\rho_l(\rho_l - \rho_v)^{-1/4}\sigma^{1/4}C_{pl}\Delta T_{sub}\frac{V_j^{1/2}}{d^{1/4}} \tag{13}$$

Experimental results from Ishigai et al. [2] and Ochi et al. [5] allowed us to validate trends predicted by relation (13). Ishigai et al. [2] obtained results with variable jet velocity, keeping the other parameters constant. We derived from Ishigai's data with a correlation coefficient of 0.9114 that $q_{sh} \sim V_j^{0.43}$ which is coherent with the relation issued from Eq. (13). In a similar way, Ochi et al. [5] presented results with variable jet diameter keeping the other parameters constant. From Ochi's data we found, with a quite better correlation coefficient of 0.9917, that $q_{sh} \sim d^{-0.34}$ that is also coherent with relation (13). No further verification by comparison with experimental data can be done because of the lack of data. From Eq. (12) a non-dimensional equation may be derived for the heat flux shoulder (relation (14)).

$$\frac{q_{sh}}{\rho_l C_{pl}\Delta T_{sub}V_j} = 0.15\left(\frac{A}{d}\right)^{1/2}\left(\frac{g}{\gamma_{tot}}\right)^{1/4} \tag{14}$$

with A (m), the Laplace length: $A = \sqrt{\frac{\sigma}{\gamma_{tot}(\rho_l-\rho_v)}}$.

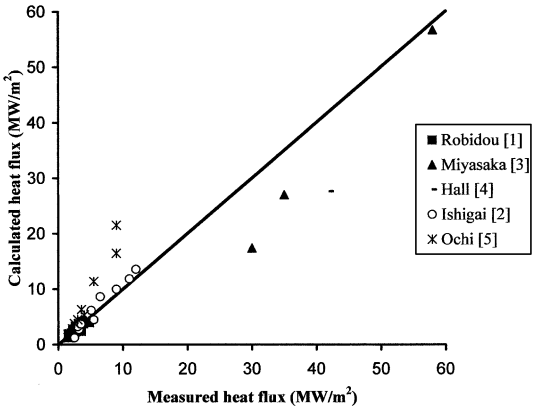

Fig. 5. Calculated shoulder heat flux versus measured heat flux at the stagnation point.

3. Modelling of the first minimum

The shape of the heat flux curve between the CHF and the heat flux shoulder results from a combination of different phenomena. Fig. 6 is a sketch of a boiling curve with the classical boiling curve and the heat flux shoulder. Two wall temperatures and one heat flux equation involved in the modelling of the first minimum have been reported on this sketch : the wall temperatures T_{wA} and T_{wB} and the equation of the heat flux exchanged by transient conduction. In order to explain how are determined T_{wA}, T_{wB} and this equation, we recall that beyond the CHF the heat flux decreases with increasing wall temperature because of increasing size

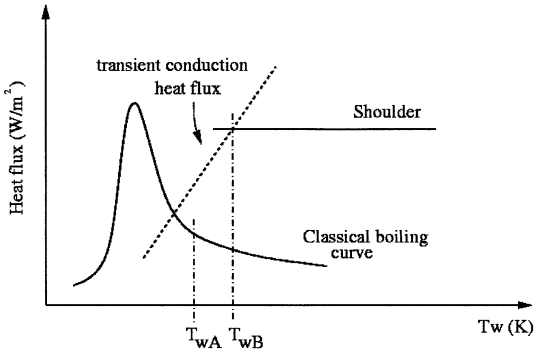

Fig. 6. Sketch for the first minimum.

of vapour spots. T_{wA} is the wall temperature for which the average radius of the vapour spots reaches the critical radius (R_{crit}). We have not been able to establish an accurate equation for predicting T_{wA}, but this temperature should be related to jet parameters such as liquid subcooling, jet velocity, nozzle size and distance to the surface. Indeed, as the jet velocity or the liquid subcooling increase, it is observed from Robidou's [1] data that T_{wA} decreases. T_{wA} will thus be considered as a parameter in this study. When the temperature of the wall is equal to T_{wA}, vapour spots are fragmented and subcooled liquid flows periodically towards the hot plate. This amount of liquid is heated up by transient conduction before being evacuated. The average heat flux ($\bar{q}$) transferred by transient conduction to the previously estimated volume of liquid (V given by Eq. (10)) during each oscillation depends on the wall temperature. T_{wB} is the wall temperature for which this heat flux $\bar{q}$ is equal to the heat flux corresponding to the shoulder. Beyond T_{wB}, the heat flux is equal to the heat flux shoulder: we supposed that the whole volume V of liquid is heated up to nearly the saturation temperature by transient conduction and is then evacuated.

The equation of the average heat flux ($\bar{q}$) evacuated by transient conduction in the liquid volume V at each oscillation and the wall temperature T_{wB} can be derived from the heat propagation equation in this volume V [11]. We consider a liquid film on the wall and the following boundary conditions.

In the following, we use for clarity the notation T_w for a wall temperature and T_i for the temperature of the liquid/wall interface at the same point.

- The initial temperature distribution function ($f(y)$) is

$$\begin{cases} T = T_i & \text{for } y = 0 \\ T = T_l & \text{for } y \neq 0 \end{cases} \tag{15}$$

  The initial time ($t = 0$) is when the liquid reaches the wall.
- For $y = \infty$, $T = T_l$.
- For any t, on plane $y = 0$, temperature is set to $T = T_i$.

T_i is the temperature of the liquid/wall interface. Carslaw and Jaeger [11] gave this temperature for a transient contact between two semi-infinite bodies with initial uniform temperatures T_l and T_w (Eq. (16)).

$$T_i = \frac{\sqrt{E_l}T_l + \sqrt{E_w}T_w}{\sqrt{E_w} + \sqrt{E_l}} \tag{16}$$

where E_l and E_w are the liquid and wall effusivities respectively $J^2/(K^2 m^4 s)$ (relation (17)).

$$E_\lambda = \rho_\lambda C_{p_\lambda} k_\lambda \tag{17}$$

with λ a subscript which may be w or l. We can notice that when the metallic wall is not oxidized, we have $T_w \sim T_i$ because the metallic wall effusivity is much more important than the liquid water effusivity. But, when the wall is oxidized T_i could be relatively smaller than the corresponding T_w and the exchanged heat flux between the liquid and the wall is also smaller than without wall oxidation.

The equation of the average heat flux ($\bar{q}$) evacuated by transient conduction during an oscillation period (τ given by Eq. (8)) is determined by considering a semi-infinite volume of liquid [11]:

$$\bar{q} = k_l \frac{(T_i - T_l)}{\sqrt{\pi \alpha_l \tau}} \tag{18}$$

with k_l the thermal conductivity of the liquid (W/(m K)), α_l the liquid thermal diffusivity (m^2/s). To validate Eq. (18) of $\bar{q}$, we consider the experimental values of T_{wB} and the corresponding heat fluxes. We consider also the experimental values of T_{wA} and the corresponding heat fluxes but only when T_{wA} is the wall temperature for which the classical boiling curve cuts the transient conduction heat flux curve. We calculate the corresponding T_{iA} and T_{iB} using Eq. (16) ($k_w = 55$ W/(m K)) and finally plot the heat flux calculated from Eq. (18) against the experimental one. The result is shown in Fig. 7. The experimental heat fluxes corresponding to T_{wA} are matched with a relative error of 23.61% and 33.96% of deviation by Eq. (18). Likewise the experimental heat fluxes corresponding to T_{wB} are matched with a relative error of 14.14% and 14.54% of deviation by Eq. (18).

For the prediction of T_{wB} we consider the same heat propagation equation between two parallel planes in a

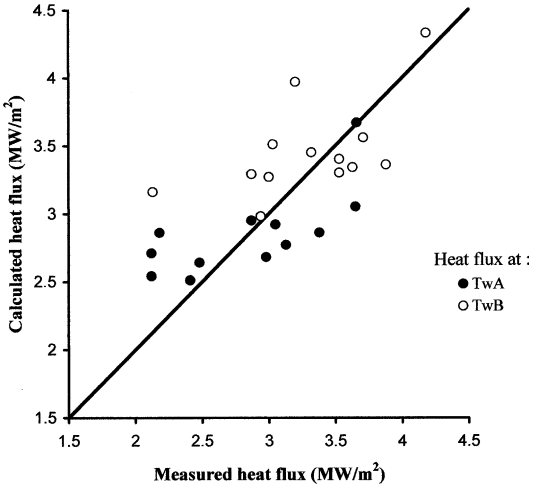

Fig. 7. Calculated average heat flux exchanged by transient conduction (Eq. (18)) versus corresponding experimental heat flux at T_{wA} and at T_{wB}.

liquid film of finite thickness δ_l. The boundary conditions are the same as previously except that for $y = \delta_l$ at any t the heat flux is zero: an isolated plane boundary condition. The solution of the heat propagation equation with this boundary conditions is given by Carslaw and Jaeger [11]:

$$T = T_i + \frac{4(T_l - T_i)}{\pi} \sum_{n=0}^{\infty} \frac{1}{(2n+1)} e^{-\alpha(2n+1)^2\pi^2 t/4\delta_l^2} \times \sin\left[\frac{(2n+1)\pi y}{2\delta_l}\right] \quad (19)$$

We assume that T_{wB} is reached when the volume V of liquid which penetrates into the vapour stores enough energy during a period to raise its average temperature from T_l to T_{sat}. The hachured area in Fig. 8 is proportional to the energy stored by a liquid layer of thickness δ_l during a time $t = \tau$. When this amount of energy balances that required to heat up the entire liquid layer to saturation temperature, we have

$$\int_0^{\delta_l} \rho_l C_{pl}(T - T_l)\,dy = \rho_l C_{pl}(T_{sat} - T_l)\delta_l \quad (20)$$

Using the solution (19) for T and integrating versus y yields to relation (21) for T_{iB}:

$$(T_{iB} - T_l) = \frac{\Delta T_{sub}}{1 - \sum_{n=0}^{\infty} \frac{8}{(2n+1)^2\pi^2} e^{-\alpha(2n+1)^2\pi^2\tau/4\delta_l^2}} \quad (21)$$

We evaluate the liquid thickness δ_l by postulating that the liquid spreads over a section of radius equal to $\beta \times$ the critical bubble radius. β is an adjustable parameter evaluated from Robidou's data. We found $\beta \simeq 2/3$.

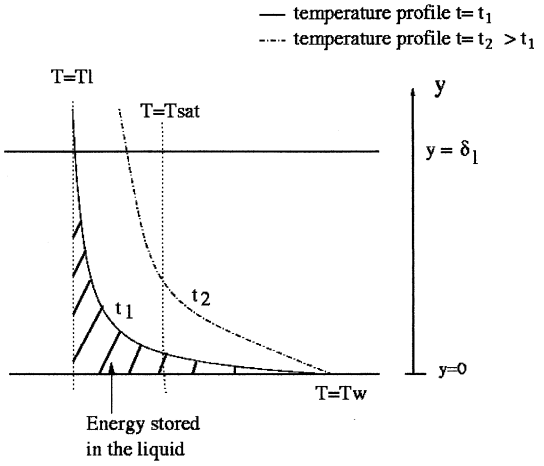

Fig. 8. Sketch of the energy stored in the liquid depending on time.

$$\delta_l = \frac{\text{displaced volume of liquid}}{\text{spreading surface}} = \frac{0.225}{V_j}\sqrt{\frac{\sigma d}{(\rho_l - \rho_v)}} \quad (22)$$

To validate relation (21), we consider the five first terms of the equation. We verify that this sum truncation led to negligible variations of about 0.2% on the value of $T_{iB} - T_l$. A good agreement with Robidou's [1] data has been reached. The result is reported in Fig. 9 and the average error is about 10% with 4% deviation. Furthermore in accordance with Eq. (16), if we consider the temperature of the liquid/wall interface T_{iB}, the corresponding wall temperature T_{wB} will be higher if the metallic wall surface is oxidized than if it is not. This trend is confirmed by experimental data reported in Fig. 10. Indeed, we suppose that the wall surface oxidation occurs at high temperature and thus the surface is oxidized when the wall temperature decreases.

This physical explanation of the boiling mechanism between the CHF and the heat flux shoulder explains the different shapes of boiling curve observed from Robidou's [1] data. A sketch of these different shapes of boiling curves is given in Fig. 11. These shapes depend on the value of T_{wA}.

- If $T_{wA} \geqslant T_{wB}$, the corresponding boiling curve is the dashed one in Fig. 11. Bubbles reach their critical radius when the wall temperature is high enough to heat up the liquid volume V to the saturation temperature during an oscillation period. For wall tempera-

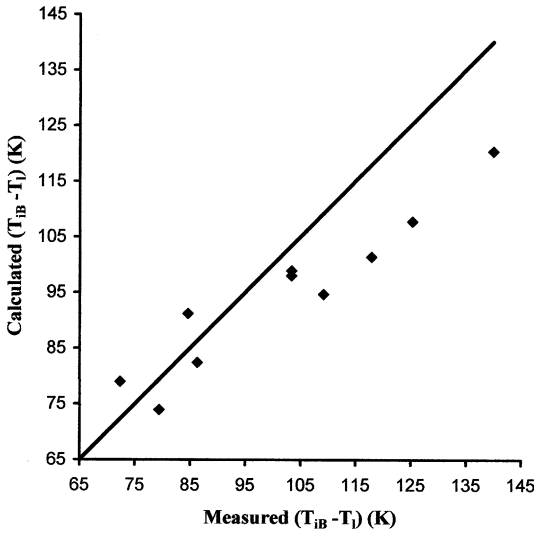

Fig. 9. Calculated temperature difference ($T_{iB} - T_l$) by Eq. (21) versus measured ($T_{iB} - T_l$).

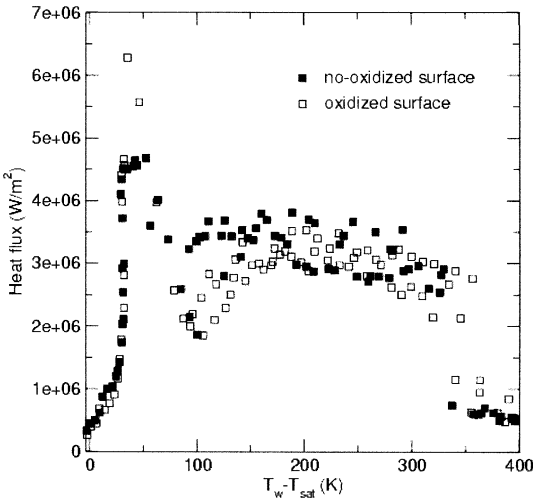

Fig. 10. Sketch of different shapes of the boiling curve between the CHF and the heat flux shoulder (Robidou [1] $V_j = 0.9$ m/s and $\Delta T_{sub} = 13.5$ K).

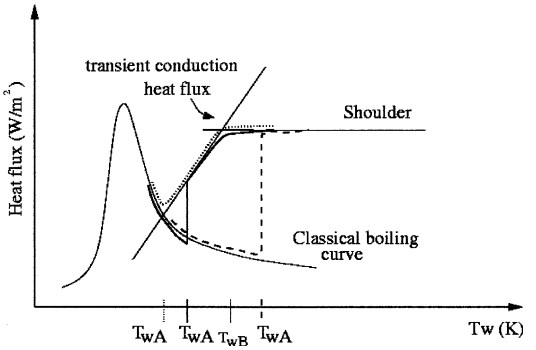

Fig. 11. Sketch of different shapes of the boiling curve between the CHF and the heat flux shoulder.

tures smaller than T_{wA}, the average heat flux is given by the classical boiling curve and for temperatures higher than this temperature the heat flux corresponds to the heat flux shoulder.

- If $T_{wA} \leqslant T_{wB}$, the corresponding boiling curves are the continuous and dotted lines in Fig. 11 and these cases are illustrated in Figs. 12 and 13 by Robidou's experimental boiling curves. When bubbles reach their critical radius, the wall temperature is not sufficient to heat up the entire liquid volume V to the saturation temperature during an oscillation period. For wall temperatures smaller than T_{wA}, the average heat flux is given by the classical boiling curve and for wall temperatures higher than T_{wA} the heat flux is limited by the transient conduction phenomenon.

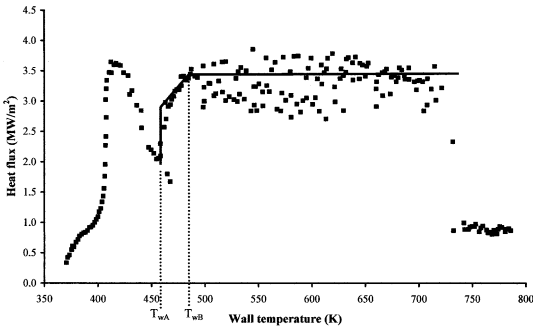

Fig. 12. Illustration of the shape described with the continuous line of Fig. 11 (Robidou [1] $V_j = 0.8$ m/s and $\Delta T_{sub} = 16$ K).

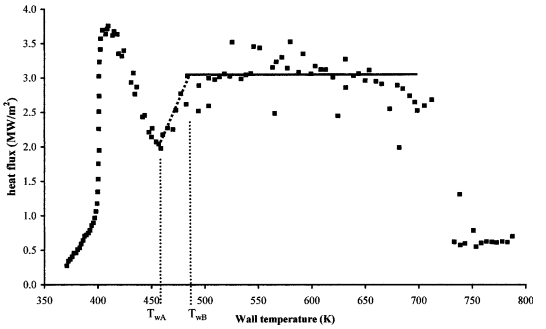

Fig. 13. Illustration of the shape described with the dotted line of Fig. 11 (Robidou [1] $V_j = 0.73$ m/s and $\Delta T_{sub} = 13.5$ K).

4. Modelling of the minimum film boiling

For wall temperatures higher than the temperature corresponding to the minimum film boiling, the heat flux shoulder disappears: the subcooled liquid does no longer wet the wall and a stable vapour layer isolates the hot plate.

In order to characterize this transition between the heat flux shoulder and the film boiling regime, we are looking for a criterion based on v_g^*. v_g^* is the critical velocity of the vapour issued from the liquid evaporation at the liquid/vapour interface beyond which this interface is stable and film boiling occurs. Kutateladze and Styrikovich [12] defined such a hydrodynamic stability criterion, but his studies on heat transfer were carried out with non-condensable bubbles emitted through a porous plate. Kutateladze and Malenkov [13] showed that, for a regime with important mixing on the wall because of gas emergence, heat transfer due to gas emission is similar to heat transfer observed in nucleate boiling. In the heat flux shoulder region, the main exchanges are also due to liquid convection and not to evaporation. From this analysis, we assume that Kutateladze's hydrodynamic stability criterion is adapted to our problem. Kutateladze and Styrikovich [12] showed

that the stability of the gas layer is linked to a competition between the two following effects: the gravity force and the aerodynamic effects of gas flowing with the velocity v_g. Similarly we write that under an impinging jet, a stable vapour film regime exists if the force linked to the aerodynamic effect due to the vapour flow ($F^a \sim \rho_v v_g^2 (\frac{\sigma}{\gamma_{tot}(\rho_l-\rho_v)})^{1/2}$) is greater than the total acceleration force ($F^\gamma \sim \rho_l \gamma_{tot} (\frac{\sigma}{\gamma_{tot}(\rho_l-\rho_g)})$). v_g is the velocity of the vapour issued from the liquid evaporation at the liquid/vapour interface. Assuming these two forces are equal and considering the same correlation as Kutateladze and Styrikovich [12], we find an expression for the critical gas emergence velocity (v_g^* given by Eq. (23)).

$$\frac{v_g^* \sqrt{\rho_v}}{(\gamma_{tot}\sigma\rho_l)^{1/4}} \simeq M^{*2/3} \tag{23}$$

with M^* a number analogous to the Mach number (Eq. (24))

$$M^* = \frac{\left(\frac{\sigma\gamma_{tot}}{(\rho_l-\rho_v)}\right)^{1/4}}{\sqrt{\frac{P}{\rho_v}}} \tag{24}$$

In stable film boiling regime, the exchanged heat flux is mainly a conduction heat flux through the vapour layer. We assume that the liquid at the liquid/vapour interface is mainly heated up by convection and only a small part is evaporated to produce the vapour flow. To establish a relation for the minimum film boiling heat flux (q_{MFB}), we postulate that the velocity of the liquid heated by convection is proportional to the critical vapour velocity v_g^* with K'' a coefficient of proportionality. The vapour is thus considered to entrain the liquid at the interface. So, the minimum film boiling heat flux may be written as

$$q_{MFB} = \underbrace{\rho_v h_{lg} v_g^*}_{\text{liquid evaporation}} + \underbrace{\rho_v C_{pl} \Delta T_{sub} K'' v_g^*}_{\text{liquid heating}} \tag{25}$$

By introducing the relation (23) into Eq. (25) and fitting K'' from the 29 experimental results of Robidou [1], we get Eq. (26). We find an average value for K'' of 0.075 with a deviation of 0.019.

$$q_{MFB} = \rho_v^{5/6} \frac{(\gamma_{tot}\sigma)^{5/12}\rho_l^{1/4}}{(\rho_l-\rho_v)^{1/6}P^{1/3}} h_{lg}\left(1 + \frac{0.075\rho_l}{h_{lg}\rho_v} C_{pl}\Delta T_{sub}\right) \tag{26}$$

Eq. (26) may be written in a non-dimensional manner as

$$\frac{q_{MFB}}{\rho_l V_j h_{fg}(1+0.075Ja)} = \sqrt{\frac{\rho_v}{\rho_l}}\sqrt{\frac{A}{d_h}}\left(\frac{g}{\gamma_{tot}}\right)^{1/4} M^{*2/3} \tag{27}$$

with M^* given by Eq. (24), $A = \sqrt{\frac{\sigma}{\gamma_{tot}(\rho_l-\rho_v)}}$, the Laplace length and Ja, the Jacob number, defined by Eq. (28).

$$Ja = \frac{C_{pl}\Delta T_{sub}}{h_{fg}} \tag{28}$$

Experimental data and correlations for the minimum film boiling heat flux in impinging jet experiments have been published by Ishigai et al. [2] and Ochi et al. [5]. Ishigai et al. [2] established the correlation (29) and Ochi et al. [5] the correlation (30).

$$q_{MFB} = 5.4 \times 10^4 (1 + 0.527\Delta T_{sub}) V_n^{0.607} \tag{29}$$

$$q_{MFB} = 3.18 \times 10^5 (1 + 0.383\Delta T_{sub}) \left(\frac{V_n}{d}\right)^{0.828} \tag{30}$$

where V_n (m/s) is the jet velocity at the nozzle exit and d the hydraulic diameter (in mm). To compare Eq. (26) to Eqs. (29) and (30), we rewrite Eq. (26) introducing thermal properties of water and neglecting the gravitational acceleration compared to the jet acceleration.

$$q_{MFB} = 1.6510^4 \frac{V_j^{0.83}}{d^{0.42}} (1 + 0.235\Delta T_{sub}) \tag{31}$$

The distances between the nozzle exit and the heated wall are 15 and 25 mm in experiments by Ishigai et al. [2] and Ochi et al. [5], respectively, and as they use vertical jets, we have $V_j \sim V_n$.

Fig. 14 compares the calculated q_{MFB} with the corresponding experimental heat flux. This comparison has been carried out with Robidou's data as well as with Ishigai's data and using either relation (26) and Eqs. (29) and (30) established by Ishigai et al. [2] and Ochi et al. [5] respectively. The comparisons of Ochi's data with relations (26), (29) and (30) have not been reported on this figure because Eqs. (26) (established in this present study) and (29) (from Ishigai's study) give results too different from Ochi's experimental data. Robidou's data for q_{MFB} are matched with a relative error of 15% and a deviation of 17% by Eq. (26), with a relative error of 55% and a deviation of 9% by Eq. (29) and finally with a relative error of 18% and a deviation of 21% by Eq. (30). Likewise, Ishigai's data of q_{MFB} are matched with a relative error of 26% and a deviation of 17% by

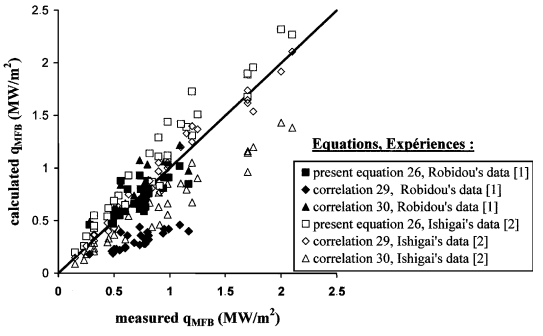

Fig. 14. Calculated q_{MFB} versus experimental q_{MFB}.

Eq. (26), with a relative error of 8.8% and a deviation of 5.8% by Eq. (29) and these experimental heat fluxes are underestimated of ~30% by Eq. (30).

The comparison of Eqs. (29)–(31) show similar dependences of q_{MFB} to liquid subcooling (ΔT_{sub}) and jet velocity (V_j). Ochi et al. [5] observed an influence of nozzle diameter on q_{MFB}. Nevertheless, this dependence is different from the one proposed by Eq. (31) ($q_{MFB} \sim d^{-0.828}$ instead of $\sim d^{-0.42}$).

5. Conclusion

The boiling curves in jet impingement configurations are different from the classical boiling curves obtained in pool or forced convection boiling systems. This holds especially for the stagnation region of the jet and transition boiling regime. Increasing the wall temperature beyond the CHF, the heat flux decreases first as it does for a classical pool boiling, but after the first minimum, it increases again towards the so-called heat flux shoulder. If the wall temperature still increases, the heat flux level remains constant until very high wall superheats before breaking abruptly down to film boiling regime.

An attempt was made to give a physically based mechanistic model of the shoulder heat flux. In accordance with the experimental observation, heat flux shoulder could be related to a transient periodic phenomenon. We assume that periodic bubble oscillations occur at the wall due to hydrodynamic fragmentation of vapour spots by the jet. At each oscillation, a certain amount of liquid wets the heated wall. This volume of subcooled liquid is heated up by conduction and is then displaced into the bulk flow by the growth of bubbles. The shoulder is reached when average liquid temperature is equal to saturation temperature. The bubble fragmentation is due to Rayleigh–Taylor instabilities, originating in the deceleration region of the jet flow. This physical mechanistic model leads to a modelling of the heat flux shoulder (Eq. (12)) which shows good agreement with the available data from the literature. This physical model is also consolidated by the fact that it supports explanations for the different shapes of boiling curves between the CHF and the heat flux shoulder. An equation for the prediction of the wall temperature T_{wB} which marks the onset of the heat flux shoulder has been established and validated. Furthermore, the heat flux corresponding to the minimum film boiling was also studied. The derived Eq. (26) matches well Robidou's and Ishigai's data.

This paper remains the first attempt to give a physical explanation of the phenomena involved in the heat flux shoulder phenomenon. The agreement of the established equations with experiments is remarkable despite the physical approximations made. The models derived should still be assessed by experimental studies on the fundamentals of two-phase dynamics near the hot surface. Such kind of experimental studies are, at that time, carried out by Bogdanic et al. [14]. They attempt to measure local data at the stagnation line of an impinging jet by means of a miniaturized optical probe which has a sensitive tip diameter of less than 1.5 μm and which is moved towards the heated hot plate by a 3D-micrometer device. By using this technique, they have already obtained basic informations notably in the shoulder region. They observed high frequencies of contact between the hot wall and the liquid and they estimated that this may confirm a mechanism like the microbubble emission boiling or the fragmentation of larger vapour spots by the jet. They expect more accurate results especially for the average vapour spots size and for contact frequencies.

Acknowledgments

This work was supported by EDF R&D Chatou. The Department of Fluid Mechanics and Heat Transfer (MFTT) is gratefully acknowledged.

References

[1] H. Robidou, Etude expérimentale du refroidissement diphasique à haute température par jet d'eau impactant, Ph.D. Thesis, University of Henri Poincaré, Nancy 1, France, 2000.
[2] S. Ishigai, S. Nakanishi, T. Ochi, Numerical simulation of multiphase flow with an elliptic oriented fractional step method, in: Proceedings of the sixth International Heat Transfer Conference, 1978, pp. 445–450.
[3] Y. Miyasaka, S. Inada, Y. Owase, Critical heat flux and subcooled nucleate boiling of in transient region between a two-dimensional water jet and a heated surface, J. Chem. Eng. Jpn. 13 (1980) 29–35.
[4] E.D. Hall, F.P. Incropera, R. Viskanta, Jet impingement boiling from a circular free-surface jet during quenching: Part 1—single-phase jet, J. Heat Transfer 123 (2001) 901–910.
[5] T. Ochi, S. Nakanishi, M. Kaji, S. Ishigai, Multi-phase and Heat Transfer III. Part A: Fundamentals—Cooling of a Hot Plate with an Impinging Circular Water Jet, Elsevier Science Publishers B.V., Amsterdam, 1984.
[6] H. Robidou, H. Auracher, P. Gardin, M. Lebouché, Controlled cooling of a hot plate with a water jet, Exp. Thermal Fluid Sci. 26 (2002) 123–129.
[7] H. Robidou, H. Auracher, P. Gardin, M. Lebouché, Local heat transfer from a hot plate to a water jet, Heat Mass Transfer 39 (10) (2003) 861–867.
[8] K. Engelberg-Forster, R. Greif, Heat transfer to a boiling liquid—mechanism and correlation, J. Heat Transfer Trans. ASME (1959) 42–52.
[9] G.I. Taylor, The instability of liquid surfaces when accelerated in a direction perpendicular to their plane,

Proceeding Royal Society of London, London, England, 1950, p. 192.
[10] S. Chandrasekhar, Hydrodynamic and Hydromagnetic Stability, Clarendon Press, Oxford, 1968.
[11] H.S. Carslaw, J.C. Jaeger, Conduction of Heat in Solids, second ed., Clarendon Press, Oxford, 1986.
[12] S.S. Kutateladze, M.A. Styrikovich, Hydrodynamics of gas–liquid systems, Moscow Energia (1976).
[13] S.S. Kutateladze, I.G. Malenkov, Boiling and bubbling heat transfer under the conditions of free and forced convection, in: Proceedings of the sixth International Heat Transfer Conference, Toronto, Canada.
[14] L. Bogdanic, H. Auracher, P. Gardin, Two-phase structure above hot surfaces in jet impingement boiling, in: 3rd European–Japanese Two Phase Group Meeting, Certosa di Pontignano, September 21–27, 2003.